




## ORIGINAL ARTICLE

# Selective perforant-pathway atrophy in Huntington disease: MRI analysis of hippocampal subfields

Pierre Wibawa<sup>1,2,3</sup>  | Mark Walterfang<sup>1,2,4</sup> | Charles B. Malpas<sup>1,2</sup>  |  
Yifat Glikmann-Johnston<sup>3</sup> | Govinda Poudel<sup>5</sup> | Adeel Razi<sup>3</sup> | Anthony J. Hannan<sup>4</sup> |  
Dennis Velakoulis<sup>1,2,4</sup> | Nellie Georgiou-Karistianis<sup>3</sup> 

<sup>1</sup>Neuropsychiatry, Royal Melbourne Hospital, Parkville, Victoria, Australia

<sup>2</sup>Melbourne Neuropsychiatry Center, University of Melbourne, Parkville, Victoria, Australia

<sup>3</sup>School of Psychological Sciences and Turner Institute for Brain and Mental Health, Monash University, Clayton, Victoria, Australia

<sup>4</sup>Florey Institute of Neuroscience and Mental Health, University of Melbourne, Parkville, Victoria, Australia

<sup>5</sup>Mary Mackillop Institute for Health Research, Australian Catholic University, Fitzroy, Victoria, Australia

## Correspondence

Pierre Wibawa, Neuropsychiatry, Royal Melbourne Hospital, Parkville, VIC 3050, Australia.

Email: [pierre.wibawa@gmail.com](mailto:pierre.wibawa@gmail.com)

## Funding information

CHDI Foundation Inc., Grant/Award Number: A-3433; National Health and Medical Research Council, Grant/Award Number: 606650

## Abstract

**Introduction:** While individuals with Huntington disease (HD) show memory impairment that indicates hippocampal dysfunction, the available literature does not consistently identify structural evidence for involvement of the whole hippocampus but rather suggests that hippocampal atrophy may be confined to certain hippocampal subregions.

**Methods:** We processed T1-weighted MRI from IMAGE-HD study using FreeSurfer 7.0 and compared the volumes of the hippocampal subfields among 36 early motor symptomatic (symp-HD), 40 pre-symptomatic (pre-HD), and 36 healthy control individuals across three timepoints over 36 months.

**Results:** Mixed-model analyses revealed significantly lower subfield volumes in symp-HD, compared with pre-HD and control groups, in the subicular regions of the perforant-pathway: presubiculum, subiculum, dentate gyrus, tail, and right molecular layer. These adjoining subfields aggregated into a single principal component, which demonstrated an accelerated rate of atrophy in the symp-HD. Volumes between pre-HD and controls did not show any significant difference. In the combined HD groups, CAG repeat length and disease burden score were associated with presubiculum, molecular layer, tail, and perforant-pathway subfield volumes. Hippocampal left tail and perforant-pathway subfields were associated with motor onset in the pre-HD group.

**Conclusions:** Hippocampal subfields atrophy in early symptomatic HD affects key regions of the perforant-pathway, which may implicate the distinctive memory impairment at this stage of illness. Their volumetric associations with genetic and clinical markers suggest the selective susceptibility of these subfields to mutant Huntingtin and disease progression.

## KEYWORDS

hippocampal subfields, hippocampus, Huntington disease, memory, MRI

Senior authors Dennis Velakoulis and Nellie Georgiou-Karistianis contributed equally to this work.

This is an open access article under the terms of the [Creative Commons Attribution-NonCommercial-NoDerivs](https://creativecommons.org/licenses/by-nc-nd/4.0/) License, which permits use and distribution in any medium, provided the original work is properly cited, the use is non-commercial and no modifications or adaptations are made.

© 2023 The Authors. *European Journal of Neurology* published by John Wiley & Sons Ltd on behalf of European Academy of Neurology.

## INTRODUCTION

Huntington disease (HD) is an inherited neurodegenerative disorder, arising from an unstable trinucleotide CAG repeat expansion in the *huntingtin* (Htt) gene. The typical diagnosis of HD is marked by the presence of choreiform movements in middle age, accompanied by an array of dysexecutive neurocognitive and behavioral symptoms [1]. Although these clinical manifestations are commonly attributed to the frontostriatum, longitudinal studies have revealed widespread brain and cognitive changes that predate the motor onset, and that are not frontostriatally mediated [2, 3]. In particular, a significant body of work has implicated hippocampal involvement in HD [4].

Many facets of hippocampal dysfunction are commonly observed in early HD [4–7]. Notably, successive studies both in human and mouse models have reported visuospatial memory deficit that is analogous and hippocampal-mediated [4]. This cognitive correlate presents as a promising measure for translating findings from animal models to human in HD as it is also associated with motor onset and disease progression [6, 8]. In contrast, whole hippocampal atrophy has not been identified consistently in the early stages of HD, but it is apparent and accelerated in the middle to late symptomatic stages [4, 5, 9]. Given the discrepancy between the hippocampal impairment and structural involvement in early HD, hippocampal atrophy may be confined to certain subfields, and may not be apparent when measured as a whole.

Several studies have evaluated the hippocampal subregions in HD [5, 9, 10]. In MRI surface analyses, atrophy of medial and posterior regions has been reported in early HD [5, 9]. Postmortem studies have shown neuronal loss in the subiculum and the body of cornu ammonis (CA) 1 [10, 11]. Interpretation of these studies, however, is limited by the omission of key hippocampal subfields, specifically those that form the main hippocampal connection, the perforant-pathway (Figure 1) [12]. Moreover, the neural correlate of visuospatial memory implicates certain subfields in the perforant-pathway. In a pioneering discovery by O'Keefe [13], the place cells, which specify the subject's location within an environment, have been described in the dentate gyrus (DG) and CA of the rat hippocampus. Successive studies have found other spatial learning cells, including head-direction, spatial-view, and grid cells, in the presubiculum [14–16]. Additionally, these cells are physiologically regulated by the inhibitory cells in the hippocampal molecular layer (ML). While these findings are derived largely from animal models during navigational tasks, virtual simulation of the same experimental conditions in humans have corroborated the involvement of the same subfields [17]. Likewise, several virtual simulation studies have reported poor navigational performance in pre-motor symptomatic (pre-HD) and early symptomatic HD (symp-HD), which posits the selective vulnerability of hippocampal subfields that comprise spatial learning cells to the neurodegenerative process in early HD [7, 8].

Recent advances in MRI segmentation techniques have offered in vivo automated volumetric analysis of the hippocampal subfields.

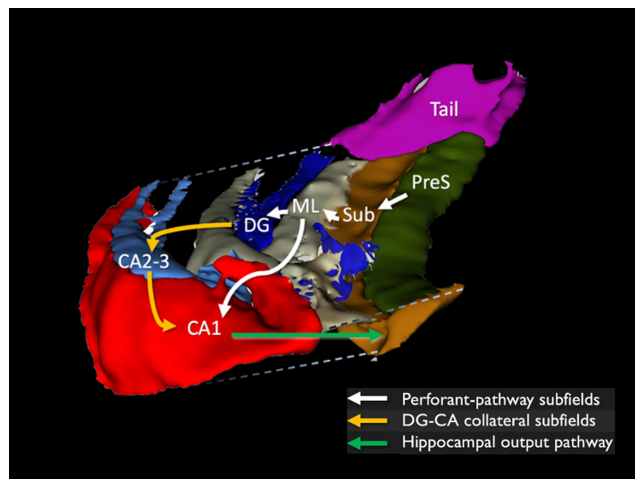


**FIGURE 1** The hippocampal perforant-pathway. The hippocampal afferent (white arrows) from the entorhinal cortex projects to the presubiculum and subiculum, perforates through the border of the subiculum and CA1, and synapses within the molecular layer of the dentate gyrus (DG) and cornu ammonis (CA). The pathway continues with the collateral connections in the DG granular and CA pyramidal regions (yellow arrows), where the hippocampal efferent projects its main output (green arrow) back to the subiculum. CA, cornu ammonis; DG, dentate gyrus; ML, molecular layer; PreS, presubiculum; Sub, subiculum.

We obtained data from the IMAGE-HD longitudinal study to compare the volumes of 12 hippocampal subfields and their annual rate of change among healthy individuals and compared these volumes to pre-HD and early symp-HD individuals. In the combined HD group, we further clustered the hippocampal subfields by their volumetric changes, and also evaluated the subfield volumes for associations with HD genetic and clinical measures. We hypothesized that the subfields comprising the perforant-pathway and involved in visuospatial memory will have significantly greater volume reductions than in other subfields and that these changes would correlate with the measures of clinical severity in HD.

## METHODS

### IMAGE-HD cohort

A total of 112 participants from the IMAGE-HD study in 2008–2009 were included in this analysis [18]. The cohort included 36 early symptomatic HD (symp-HD), 40 presymptomatic HD (pre-HD), and 36 healthy control individuals. MRI scanning and clinical assessments were conducted for each individual in three timepoints: at baseline, 18 months, and 36 months. Of these visits, 96 participants (85.6%) completed longitudinal scans and assessments (2 timepoints,  $n=18$ ; 3 timepoints,  $n=78$ ). This study was approved by the Monash University Human Research Ethics Committees, and each participant provided written informed consent.

## Clinical characteristics

Diagnostic assessments were carried out in a specialist HD clinic in Victoria, Australia. In addition to having a formal clinical diagnosis, and  $\geq 39$  CAG repeat length, the case groups were differentiated by Unified Huntington's Disease Rating Scale (UHDRS) total motor score of  $>5$  for symp-HD and  $\leq 5$  for pre-HD [3]. Self-reported onset of first motor symptoms was collected in the symp-HD and estimated years to onset was calculated for the pre-HD group [19]. We also calculated the disease burden score (DBS):  $\text{age} \times (\text{CAG} - 35.5)$  [3]. Healthy controls were matched to pre-HD individuals for age, gender, and premorbid intelligence quotient (IQ). Scores on the symbol digit modalities test (SDMT) were also included. A summary of demographic and clinical characteristics is shown in Table 1.

## MRI acquisition

T1-weighted images were acquired on a Siemens Magnetom Trio Tim System 3 Tesla scanner with a 32-channel head coil at the Royal Children's Hospital, Victoria, Australia. Sequence parameters comprised 192 slices with  $0.9 \times 0.8 \times 0.8$  mm image resolution,  $320 \times 320$  field of view, inversion time of 900 ms, echo time of 2.59 ms, recovery time of 900 ms, and  $9^\circ$  flip angle.

## Image preprocessing

### Automated segmentation of hippocampal subfields

All T1 images were included after visual inspection for artefact. Automated brain segmentation was carried out in FreeSurfer version 7.0. These procedures are well-validated and have been detailed at <https://surfer.nmr.mgh.harvard.edu/fswiki/FreeSurferMethod>

**TABLE 1** Clinical variables and demographics.

	Healthy control (n = 36)	Pre-HD (n = 40)	Symp-HD (n = 36)
Age (years)*	42.7 (13.9)	41.8 (9.9)	51.9 (9.4)
Sex	24 F, 12 M	24 F, 16 M	15 F, 21 M
CAG repeat	–	42.2 (1.9)	43.0 (2.4)
Disease burden score*	–	267.4 (56.5)	382.9 (67.2)
UHDRS motor*	–	0.8 (1.2)	19.4 (12.5)
SDMT*	56.3 (10.1)	52.5 (8.8)	35.8 (11.8)
Premorbid IQ	118.0 (9.7)	116.9 (11.2)	113.7 (11.6)

Note: All variables are shown as mean  $\pm$  SD, except for CAG repeat (median  $\pm$  SD) and gender.

Abbreviations: F, female; HD, Huntington disease; IQ, intelligence quotient; M, male; pre-HD, pre-symptomatic HD; SDMT, Symbol Digit Modalities Test; symp-HD, symptomatic HD; UHDRS, Unified Huntington Disease Rating Scale.

\* $p < 0.001$  for symp-HD vs. pre-HD and symp-HD vs. control.

dsCitation. For cross-sectional subjects, T1-weighted scans underwent affine transformation to MNI305 space and skull stripping. Segmented volumetric structures were labeled based on normalized intensity and neighboring constraints. For individual with scans from multiple timepoints, a longitudinal pipeline was used to reduce the within-subject variability [20]. A within-subject template was created for each subject using robust, inverse consistent registration from the common information in each timepoint, which yielded an identical total intracranial volume (TIV) for the individual. The longitudinal scans were then processed according to the cross-sectional pipeline using the within-subject template, thereby increasing segmentation reliability. Subsequently, automated segmentation algorithm of hippocampal subfields was applied to cross-sectional and longitudinal processed data. This algorithm, based on Bayesian inference, utilized image intensities and probabilistic atlas from 7 Tesla *ex vivo* MRI of 15 subjects and 1.5 Tesla *in vivo* MRI with 1 mm resolution of 39 subjects [21]. The examined hippocampal subfields were parasubiculum, presubiculum, subiculum, CA1, CA2-3, CA4, granule, and molecular layer of DG, molecular layer of hippocampus (ML), hippocampal-amygdala transitional area (HATA), fimbria, tail, and fissure.

Quality control procedures were applied by examining volumetric outliers within each group ( $\geq 2.98$  SD) and visually inspecting for the segmentation accuracy [22]. No manual modification or data exclusion was necessary. A FreeSurfer-processed template of a random normal subject was 3D-rendered using Slicer software to illustrate the pair-group mean volumetric differences [23].

## Statistical analysis

Data were analyzed using jamovi version 1.6, which was based on R version 4.1.2 (2021). Baseline demographic data and clinical measures in pre-HD, symp-HD, and healthy control groups were compared using ANOVA, Fisher's exact, Mann-Whitney U, or independent t-test according to the data distribution. All volumetric analyses were corrected for false discovery rate (FDR) at 5% (see Supplemental Tables A–C).

To compare group differences in subfield volumes, we used separate general linear mixed-effect models (GLMM) for each subfield with the volume as dependent variable. Group was entered as an independent variable, along with baseline age, days from baseline scan (timepoint), TIV, and sex. Random intercepts and slopes were specified for each participant. To investigate the group differences in annual rate of volume change, we used a general linear model (GLM) to include the regression slope of within-subject subfield volumes over the longitudinal timepoints as the dependent variable and the group as an independent variable, and covarying for baseline age, TIV, and sex.

Using principal component analysis, we examined for any clustering of the hippocampal subfield volumes that was intrinsic to HD. The subfields volumes in the pre-HD and symp-HD groups were combined, adjusted for TIV, and standardized for longitudinal repeated

measures using the proportion of maximum scaling method [24]. Components from standardized volumes were then derived using the oblimin method with the loading size of  $\geq 0.4$  and Eigenvalue of  $>1$ . The sum of the component loadings and the subfields volumes were used as the dependent variables and subsequently analyzed with the equivalent GLMM and GLM that was applied to the individual subfield.

To assess for associations with the clinical measures, UHDRS motor score in the symp-HD, estimated years to motor onset in the pre-HD, and CAG repeat length, DBS, and SDMT in the combined symp-HD and pre-HD group were individually included as a predictor of the subfields in GLMM with the subject's intercept and slope as random effect. UHDRS, CAG repeat, and SDMT models were adjusted for age, TIV, and scan timepoints. DBS and estimated motor onset were adjusted for TIV and scan timepoints.

## RESULTS

### Demographics and clinical characteristics

Symp-HD group were significantly older, had greater DBS, higher UHDRS total motor score, and lower SDMT score than pre-HD (Table 1). CAG repeat length in the pre-HD and symp-HD participants

ranged from 39 to 50. Mean estimated time to onset in pre-HD was  $9.3 \pm 7.5$  years and the duration since first motor symptoms in symp-HD was  $3.4 \pm 1.9$  years. Pre-HD participants had lower SDMT scores than the healthy controls, but their age, sex, and premorbid IQ were not significantly different.

### Group comparison of hippocampal subfield volumes

The group volume comparisons, which were adjusted for age, multiple scan timepoints, TIV, and sex, are shown in Figure 2 and Table 2. Whole hippocampal volumes were smaller bilaterally in the symp-HD compared to pre-HD and control groups. In the subfields, bilateral atrophy was seen in the presubiculum and tail of symp-HD when compared to pre-HD, and in the subiculum when compared to controls. The greatest volume differences were seen between symp-HD and controls in the right presubiculum, and between symp-HD and pre-HD in the left presubiculum. There were other unilateral hippocampal subfields reductions in symp-HD compared to pre-HD in the left CA4 and DG, compared to controls in the right DG and tail, and compared to both groups in the right ML. Enlarged right fissure in symp-HD, when compared to controls, accompanied the atrophy in the subicular, ML, and DG regions. Volumes of whole hippocampus or hippocampal subfields did not differ significantly between pre-HD and control groups.

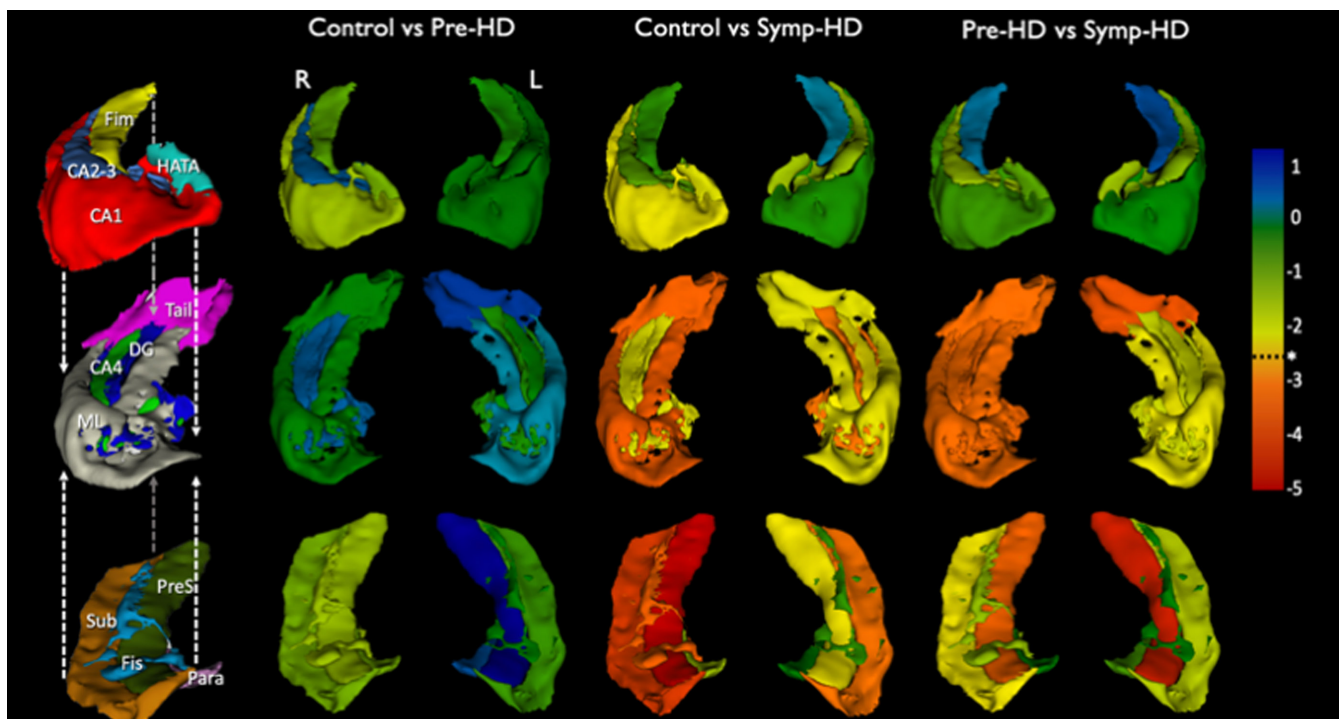


**FIGURE 2** Volume comparisons of hippocampal subfields across groups. Group differences in hippocampal subfield volumes are shown in t-scores color scales (blue=higher volume in the latter group, yellow-green=lower volume, orange-red=significantly lower volume with  $*pFDR < 0.05$ ). Volume differences were adjusted for multiple scan timepoints, age, sex, total intracranial volume, and the subject's volume slope and intercept. The illustrated subfields, as labelled on the left, are separated vertically into three sections and aligned with dashed lines. CA, cornu ammonis; DG, dentate gyrus; FDR, false discovery rate; Fim, fimbria; Fis, fissure; L, left; ML, molecular layer; Para, parasubiculum; Pre-HD, pre-symptomatic Huntington disease; PreS, presubiculum; R, right; Sub, subiculum; Symp-HD, symptomatic Huntington disease.

**TABLE 2** Group comparisons of hippocampal subfield volumes.

Subfields	Healthy control	Pre-HD	Symp-HD	Group comparisons (t-score)
<b>Right</b>				
Whole hippocampus	3782.3 (3675.3–3889.3)	3714.6 (3613.7–3815.4)	3485 (3376–3593.9)	C > S (–3.731), P > S (–2.957)
Parasubiculum	62.9 (58.9–67)	59.3 (55.5–63.1)	57.8 (53.7–61.9)	–
Presubiculum	319.3 (306.6–332)	305.1 (293.2–316.9)	278 (265.1–290.8)	C > S (–4.345), P > S (–2.966)
Subiculum	443.2 (427.3–459)	428.5 (413.6–443.4)	400.1 (384–416.2)	C > S (–3.637)
CA1	692 (667.7–716.3)	664 (641.1–686.9)	648.2 (623.5–673)	–
CA2-3	244.4 (233.6–255.2)	248 (237.8–258.2)	235.1 (224.1–246.1)	–
CA4	309.1 (296.2–322.1)	313.3 (301.2–325.5)	287.5 (274.3–300.6)	P > S (–2.766)
Dentate gyrus	342.2 (329.5–354.9)	346.2 (334.2–358.2)	320 (307–333)	P > S (–2.841)
Molecular layer	640.1 (618.3–661.8)	633.7 (613.2–654.2)	590.2 (568.1–612.4)	C > S (–3.075), P > S (–2.756)
Fimbria	76.2 (69.9–82.5)	71.7 (65.9–77.6)	72.6 (66.2–78.9)	–
Fissure	161.4 (151.9–170.8)	172.1 (163.4–180.8)	182.6 (173.1–192)	C < S (3.017)
HATA	60.4 (57.8–63)	58.1 (55.7–60.5)	56 (53.4–58.6)	–
Tail	592.9 (568.5–617.3)	586.8 (563.9–609.6)	538.5 (513.7–563.2)	C > S (–2.989), P > S (–2.741)
<b>Left</b>				
Whole hippocampus	3572.4 (3468.4–3676.5)	3576.6 (3478.8–3674.5)	3365.7 (3259.9–3471.5)	C > S (–2.666), P > S (–2.803)
Parasubiculum	62.8 (58.7–66.9)	64.5 (60.7–68.4)	61.7 (57.5–65.8)	–
Presubiculum	317.5 (305.3–329.8)	329.8 (318.4–341.3)	294.6 (282.2–307)	P > S (–3.993)
Subiculum	433.7 (418–449.4)	424.3 (409.6–439.1)	402.4 (386.5–418.4)	C > S (–2.675)
CA1	637.2 (614.6–659.8)	635.1 (613.9–656.3)	625.2 (602.3–648.1)	–
CA2-3	222.5 (211.7–233.4)	221.5 (211.3–231.7)	209.6 (198.6–220.7)	–
CA4	291 (279.7–302.4)	286.6 (276–297.2)	269.6 (258.1–281.1)	–
Dentate gyrus	325.2 (313.6–336.8)	319.9 (309–330.8)	302.5 (290.7–314.3)	C > S (–2.614)
Molecular layer	606.1 (585–627.1)	606.3 (586.5–626.1)	569.4 (548–590.8)	–
Fimbria	82.4 (76.2–88.7)	79.6 (73.8–85.4)	82.6 (76.3–88.9)	–
Fissure	165.9 (155.5–176.3)	169 (159.4–178.6)	171.9 (161.5–182.4)	–
HATA	56.9 (54.4–59.5)	56.8 (54.4–59.1)	53.7 (51.1–56.3)	–
Tail	536.8 (512.1–561.5)	552.3 (529.1–575.4)	494.4 (469.4–519.5)	P > S (–3.246)

Note: Standardized mean volumes (95% confidence interval) are shown and adjusted for multiple scan timepoints, age, sex, total intracranial volume, and the subject's volume slope and intercept. Pair-group mean comparisons with  $pFDR < 0.05$  are shown in the right column.

Abbreviations: C, healthy control; CA, cornu ammonis; FDR, false discovery rate; HATA, hippocampal-amygdala transitional area; P, pre-symptomatic Huntington disease (pre-HD); S, symptomatic Huntington disease (symp-HD).

### Group comparison of annual rate of hippocampal subfield volume change

The annual rate of volume change did not differ in any of the hippocampal subfields across the groups after FDR correction (Table S1). Without the correction, symp-HD had a higher annual rate of atrophy than pre-HD and control groups in the subiculum bilaterally, left presubiculum and fissure, and right fimbria and whole hippocampus (unadjusted  $p < 0.05$ ). Compared to pre-HD, symp-HD had a higher atrophy rate in the left whole hippocampus, DG, and ML. Pre-HD group had a greater rate of left fissure enlargement than controls.

### Principal components of hippocampal subfields, their volume differences, and annual rate of change in HD

We identified five hippocampal subfield principal components in the combined pre-HD and symp-HD group. The first component comprised bilateral DG, CA4, CA3, ML, and left CA1, and the second included bilateral presubiculum, subiculum, and tail, as well as right ML and CA1. These two components accounted for 51.9% of the total variance. Based on the structural connectivity from presubiculum to CA (Figure 1), the first component formed the 'DG-CA collateral subfields' and the second formed the subicular 'perforant-pathway subfields' [12, 25]. The three additional



components, which explained an additional 29.1% of the variance and comprised HATA, fimbria, parasubiculum, and fissure, were not part of the main hippocampal pathway and were excluded from further analyses (Table S2).

Compared to pre-HD and controls, symp-HD had lower mean volume of the perforant-pathway (symp-HD  $2543.4 \pm 42.8$  vs. pre-HD  $2749.8 \pm 39.6$  vs. controls  $2777.6 \pm 42.2$ ) and DG-CA collateral subfields (symp-HD  $2398.5 \pm 43.2$  vs. pre-HD  $2541.9 \pm 40.0$  vs. controls  $2546.6 \pm 42.5$ ) (see Table S3). Annual rate of volume loss was significantly higher only in the perforant-pathway subfields of symp-HD when compared to pre-HD and controls (symp-HD  $-31.6 \pm 4.6$  vs. pre-HD  $-7.0 \pm 4.1$  vs. controls  $-8.2 \pm 4.7$ ) (see Figure 3).

### Associations of subfields with clinical variables

After adjusting for age and TIV, number of CAG repeats in the combined HD group showed significant bilateral associations with the whole hippocampus, presubiculum, ML, and tail, and the subicular perforant-pathway subfields. DBS was associated with most hippocampal structures bilaterally, except for parasubiculum, fimbria, HATA, and left fissure. In pre-HD, motor onset was associated with the left whole hippocampus and tail, and perforant-pathway subfields volume. UHDRS motor score and SDMT were not significantly associated with any of the hippocampal structures (Table 3). Further analyses for CAG, DBS, and SDMT in pre-HD and symp-HD group did not reveal any additional structural associations to the combined HD group, except for the CAG repeat in pre-HD being only associated with left tail and perforant subfields (Table S4).

## DISCUSSION

This study evaluates discrete volumes of hippocampal subfields in pre-HD and early symp-HD, given prior evidence of hippocampal-specific impairment in the early stages of HD. We report a selective reduction in subfield volumes in the symp-HD group, compared with pre-HD and controls, comprising tail, presubiculum, subiculum, DG, and right ML. Volumes of these subfields aggregate into a single principal component, which demonstrates an accelerated rate of volume loss during the early symptomatic stage and highlights the vulnerability of the afferent and subicular regions in the hippocampal perforant-pathway. Clinically, these implicated subfields are associated with the CAG repeat length, DBS, and motor onset.

Whole hippocampal atrophy in our early symp-HD cohort is consistent with previous studies [4, 9]. In contrast, we did not find any volume differences between the pre-HD and matched healthy controls in the whole hippocampus or its subfields, which adds to the variable reports of hippocampal atrophy in the pre-symptomatic stage [5, 9].

The reduced subicular volume in symp-HD compared to controls supports previous findings in a postmortem study by Braak et al. [10], who coincidentally postulate the involvement of the perforant-pathway. Although there is a trend of subicular atrophy in symp-HD when compared to pre-HD group, greater volume differences in the presubiculum, ML, and tail may specify a vulnerability that is intrinsic to HD.

The prominent presubiculum and tail atrophy in symp-HD supports our hypothesis regarding the selective involvement of subfields that mediate visuospatial memory. Deficits in visuospatial memory in early HD have been shown in human studies

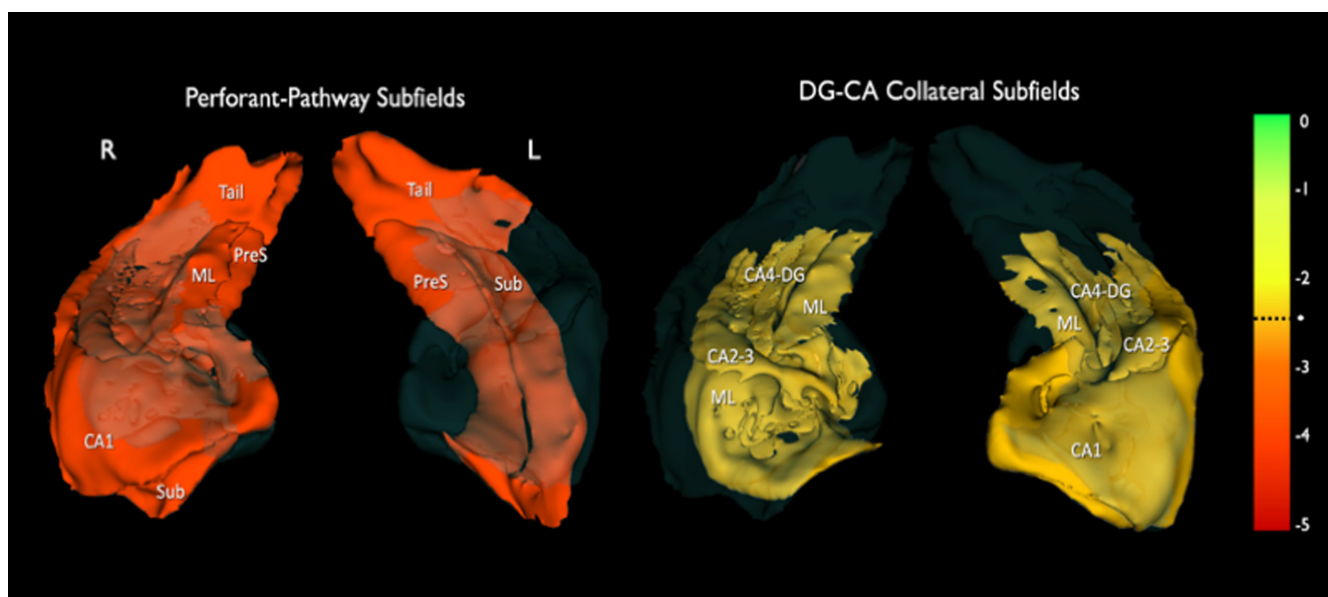


**FIGURE 3** Annual rate of atrophy in the hippocampal components between pre-symptomatic Huntington disease (pre-HD) and symptomatic Huntington disease (symp-HD) groups. Symp-HD had a greater annual rate of volume reduction than pre-HD in perforant-pathway subfields component (\* $pFDR < 0.05$ ), but not in DG-CA collateral component. The main hippocampal pathway is shown at the bottom. CA, cornu ammonis; DG, dentate gyrus; FDR, false discovery rate; ML, molecular layer; PreS, presubiculum; Sub, subiculum.

and animal models under comparable testing conditions (e.g., the virtual Morris water maze) [7, 8]. In animal models, these testing conditions elicit the physiological activation of various hippocampal spatial learning cells, such as the spatial-view, head-direction, and grid cells. These cells are postulated to exist in the human presubiculum [16, 26, 27]. In the hippocampal tail, our findings of atrophy in symp-HD is aligned with a previous study in early HD [9]. The hippocampal tail is heterogeneous, containing the caudal extension of other subfields from the hippocampal body [27, 28]. Differentiation of these subfields in the hippocampal tail is currently beyond the conventional MRI spatial resolution at clinically available field strengths such as 3T. Nonetheless, the functional interconnectivity of the hippocampal tail, presubiculum, and occipitoparietal region has been demonstrated in humans and appears to be involved in the cognitive processes of visuospatial memory [17].

Molecular layer (ML) atrophy may further contribute to the impaired spatial memory in symp-HD. This subfield is enriched with inhibitory interneurons that regulate theta rhythm, which heralds the online state of spatial learning cells during navigation [13, 29]. In HD, aberrant theta activities have been detected in the hippocampus and temporal regions, as well as correlated with cognitive performance and CAG repeats [30, 31]. Mutant *Huntingtin* (mHtt) aggregates, encoded by an elongated CAG repeat, appear readily detectable in ML [32]. Although the relationship between mHtt aggregates and ML interneuronal survival remains unclear, marked loss of inhibitory interneurons have been reported in the striatum and various cortices [33, 34]. Among the various classes of interneurons, striatal parvalbumin interneurons appear to be most affected in HD and share similar  $\gamma$ -aminobutyric acid A (GABA<sub>A</sub>) binding profiles (i.e., benzodiazepine-sensitive) to the parvalbumin interneurons in presubiculum and ML, where various spatial learning cells have been colocalized [27, 35–37].

In early HD, mHtt dysregulates endocytosis and recycling of various membrane receptors, resulting in toxic gain of function and membrane receptors alterations [38]. Within the hippocampus, the presence of mHtt aggregates has been associated with reduced GABA<sub>A</sub>, muscarinic 2 (M<sub>2</sub>), serotonin 1 (5-HT<sub>1</sub>), and alpha-adrenergic 2 ( $\alpha_2$ ) receptor densities [39–43]. Topographically, these receptors show differential distribution among the subfields in the neurologically healthy human hippocampi, including high GABA<sub>A</sub> and M<sub>2</sub> receptor affinities in presubiculum and ML, and 5-HT<sub>1A</sub> and  $\alpha_2$  affinities in ML [37, 44]. This receptor-based topography conforms with the pattern of subfield atrophy in our symp-HD individuals and lends support to the concept that there is a process of advancing pathophysiology of mHtt from membrane receptor alterations to neuronal death in the hippocampus.

The DG has been evaluated discretely in HD for its role in spatial memory, its pathogenic vulnerability to mHtt, and its capacity for neurogenesis [4]. A viral transduction of mHtt into the DG of wild-type adult mice is associated with altered gene expression in granule cells, and resulted in spatial memory impairment [45]. Maturation of DG granule cells is also regulated by inhibitory

interneurons in its molecular layer [46]. Thus, the atrophy of DG in symp-HD may arise from its molecular layer and the granule cell layer.

Collectively, the presubiculum, subiculum, tail, and right ML volume in our HD cohorts aggregate into a single component. This component corresponds to the subicular regions of the perforant-pathway and contains the hippocampal afferent that stems from the entorhinal cortex, perforates through the presubiculum and subiculum, and synapses at the ML of CA1 and DG (Figure 1). Hippocampal output originating from the efferent region (CA pyramidal and DG granule layer) also projects out to the subiculum [12]. Thus, accelerated atrophy in the subicular regions of the perforant-pathway in symp-HD involves the main hippocampal connections and may result in global hippocampal impairment.

Numerous postmortem studies in HD have reported the presence of pathogenic tau and neurofibrillary tangles in the medial temporal region [47]. The relatively older subject age in these studies compared to our cohort, however, suggests that tau may be involved in the later stages of the disease. The distribution of tau in the hippocampal subfields is unclear given the lack of systematic evaluation. A postmortem study has observed pathogenic tau staining in the CA pyramidal and DG granule cells [48]. Although the volume of the DG-CA collateral component is significantly reduced in our HD cohorts, the more prominent atrophy in the subicular perforant-pathway component may primarily diminish the connection and inhibition to the DG-CA pyramidal region, leading to deafferentation and excessive excitotoxicity [10].

CAG repeat length, which predicts the age of motor onset and the rate of functional decline, is associated with whole hippocampal, presubiculum, ML, tail, and perforant-pathway subfields volumes in our HD cohorts [49]. This association complements the pattern of hippocampal subfield atrophy in symp-HD when compared to pre-HD. Although the combination of CAG repeat and age in DBS has revealed widespread subfields associations, there is a relatively stronger relationship with the subiculum and ML, left presubiculum and tail, and subicular perforant-pathway component than the other subfields and DG-CA component. These relationships with the CAG-based measures further suggest that the hippocampal neurodegeneration in early HD may be mediated by mHtt and predominantly affect the presubiculum, subiculum, ML, tail, and subicular perforant-pathway region.

Consistent with earlier studies, we found significant associations between the posterior hippocampal region (i.e., left tail) and CAG repeat [4, 9]. Additionally, the left tail was associated with motor onset in our pre-HD group. Mutant Htt may preferentially exert greater pathogenic effect posteriorly due to its dense myelination [25, 50]. Moreover, SDMT and UHDRS motor score are not associated with the subfield volume. These measures may correlate predominantly with the frontostriatal and other cortical regions [2].

This study has several noteworthy limitations. First, the symp-HD group does not include matched healthy controls, which limits our ability to examine the relationship between the subfield volumes and

TABLE 3 Associations of hippocampal subfields volume with clinical measures in the Huntington disease groups.

Subfields	CAG repeats	DBS	Estimated motor onset	SDMT	UHDRS motor
<b>Right</b>					
Whole hippocampus	-0.232 (-0.401 - -0.064)*	-0.193 (-0.369 - -0.016)*	0.139 (-0.010-0.288)	0.039 (-0.030-0.108)	-0.017 (-0.066-0.032)
Parasubiculum	0.033 (-0.212-0.277)	-0.388 (-0.499 - -0.276)	0.123 (-0.105-0.350)	-0.052 (-0.185-0.082)	0.032 (-0.069-0.132)
Presubiculum	-0.271 (-0.473 - -0.069)*	-0.155 (-0.341-0.031)*	0.192 (-0.050-0.433)	0.027 (-0.102-0.156)	-0.022 (-0.120-0.075)
Subiculum	-0.100 (-0.290-0.090)	-0.402 (-0.567 - -0.237)*	-0.041 (-0.216-0.134)	0.051 (-0.040-0.142)	-0.052 (-0.118-0.014)
CA1	-0.144 (-0.325-0.037)	-0.279 (-0.419 - -0.140)*	0.129 (-0.025-0.283)	0.054 (-0.024-0.131)	-0.024 (-0.079-0.032)
CA2-3	-0.072 (-0.265-0.121)	-0.226 (-0.349 - -0.103)*	-0.004 (-0.154-0.147)	0.034 (-0.046-0.114)	-0.031 (-0.088-0.025)
CA4	-0.175 (-0.373-0.023)	-0.168 (-0.295 - -0.041)*	0.135 (-0.044-0.314)	0.036 (-0.049-0.121)	-0.001 (-0.061-0.060)
Dentate gyrus	-0.174 (-0.362-0.014)	-0.288 (-0.420 - -0.156)*	0.132 (-0.041-0.305)	0.046 (-0.037-0.129)	-0.015 (-0.074-0.045)
Molecular layer	-0.257 (-0.440 - -0.074)*	-0.306 (-0.435 - -0.177)*	0.158 (-0.014-0.330)	0.079 (0.003-0.156)	-0.016 (-0.071-0.038)
Fimbria	0.156 (-0.062-0.375)	-0.383 (-0.506 - -0.261)	-0.089 (-0.358-0.179)	-0.122 (-0.301-0.057)	-0.058 (-0.211-0.095)
Fissure	0.157 (-0.041-0.354)	-0.010 (-0.215-0.195)*	-0.317 (-0.570 - -0.063)	-0.184 (-0.353 - -0.016)	0.045 (-0.103-0.193)
HATA	-0.076 (-0.303-0.151)	0.251 (0.077-0.426)	0.059 (-0.149-0.266)	-0.105 (-0.264-0.054)	-0.013 (-0.140-0.113)
Tail	-0.382 (-0.58 - -0.184)*	-0.165 (-0.355-0.025)*	0.146 (-0.068-0.360)	0.044 (-0.072-0.160)	-0.014 (-0.100-0.071)
<b>Left</b>					
Whole hippocampus	-0.267 (-0.435 - -0.098)*	-0.446 (-0.569 - -0.323)*	0.212 (0.067-0.357)*	-0.031 (-0.111-0.048)	-0.032 (-0.090-0.026)
Parasubiculum	-0.013 (-0.228-0.202)	-0.137 (-0.302-0.029)	0.093 (-0.099-0.285)	-0.020 (-0.144-0.104)	-0.008 (-0.098-0.083)
Presubiculum	-0.316 (-0.506 - -0.127)*	-0.423 (-0.579 - -0.266)*	0.229 (0.027-0.432)	0.066 (-0.060-0.191)	-0.025 (-0.121-0.072)
Subiculum	-0.187 (-0.372 - -0.002)	-0.427 (-0.564 - -0.29)*	0.196 (0.036-0.355)	0.021 (-0.066-0.107)	-0.039 (-0.101-0.024)
CA1	-0.122 (-0.297-0.052)	-0.243 (-0.369 - -0.117)*	0.169 (0.020-0.319)	-0.074 (-0.172-0.024)	-0.025 (-0.085-0.035)
CA2-3	-0.122 (-0.324-0.081)	-0.205 (-0.354 - -0.057)*	-0.032 (-0.207-0.144)	-0.023 (-0.126-0.080)	-0.041 (-0.114-0.032)
CA4	-0.181 (-0.378-0.017)	-0.329 (-0.483 - -0.176)*	0.093 (-0.107-0.294)	0.001 (-0.111-0.111)	-0.058 (-0.139-0.022)
Dentate gyrus	-0.178 (-0.372-0.017)	-0.347 (-0.500 - -0.194)*	0.088 (-0.106-0.282)	-0.005 (-0.113-0.103)	-0.067 (-0.146-0.012)
Molecular layer	-0.267 (-0.450 - -0.083)*	-0.472 (-0.602 - -0.343)*	0.203 (0.043-0.364)	-0.028 (-0.111-0.055)	-0.018 (-0.080-0.043)
Fimbria	0.175 (-0.035-0.384)	-0.008 (-0.199-0.182)	0.011 (-0.229-0.251)	-0.086 (-0.241-0.070)	-0.067 (-0.192-0.058)
Fissure	0.015 (-0.206-0.236)	0.117 (-0.077-0.311)	-0.354 (-0.626 - -0.082)	0.027 (-0.156-0.210)	0.005 (-0.150-0.160)
HATA	-0.153 (-0.359-0.053)	-0.181 (-0.346 - -0.016)	0.073 (-0.114-0.259)	-0.007 (-0.138-0.123)	0.002 (-0.098-0.102)
Tail	-0.447 (-0.645 - -0.249)*	-0.462 (-0.614 - -0.311)*	0.294 (0.102-0.486)*	-0.064 (-0.223-0.095)	-0.034 (-0.120-0.053)
<b>Subfields component</b>					
Perforant subfields	-0.334 (-0.509 - -0.159)*	-0.460 (-0.585 - -0.336)*	0.233 (0.074-0.393)*	0.026 (-0.057-0.109)	-0.014 (-0.073-0.045)
DG-CA collateral	-0.267 (-0.435 - -0.098)	-0.360 (-0.479 - -0.241)*	0.126 (-0.021-0.274)	-0.016 (-0.090-0.058)	-0.027 (-0.080-0.026)

Note: Associations are shown in standardized coefficient ( $\beta$ ) with 95% confidence interval.

All models were adjusted for multiple scan timepoints, total intracranial volume, and the subject's volume slope and intercept, in addition to age in the CAG repeats, SDMT, and UHDRS models.

Abbreviations: CA, cornu ammonis; DBS, disease burden score; DG, dentate gyrus; FDR, false discovery rate; HATA, hippocampal-amygdala transitional area; SDMT, Symbol Digit Modalities Test; UHDRS, Unified Huntington Disease Rating Scale.

\*pFDR < 0.05.



the independent effect of age in healthy individuals, as well as the effect of age-gene size interaction in symp-HD. Secondly, the classification between pre-HD and symp-HD group is clinically reliant on motor symptoms. We did not find any associations between the hippocampal subfields and UHDRS motor score. Further evaluation using standardized measures that integrate MRI data and measures of motor and other neurocognitive symptoms may offer more homogeneous comparisons of hippocampal subfields across different studies in the future. Nevertheless, our post-hoc analyses using a novel HD integrated staging system have revealed comparable results to the IMAGE-HD group classification (Figure S1, Tables S5, and S6). Finally, there is a significant gap in translating the structural findings in our study as measures of visuospatial memory are not available.

In conclusion, the differential pattern of hippocampal subfield atrophy seen in our early motor symptomatic group is consistent with the known cellular pathophysiology in HD, specifically the effect of mutant *Huntingtin* on vulnerable regions in the hippocampus. Functionally, atrophy in these structures may contribute to hippocampal dysfunction, including visuospatial memory impairment, in early HD. Further cognitive and pathological evaluations of the hippocampal subfields are critical for confirming our findings. Nonetheless, automated MRI hippocampal segmentation can be readily implemented and provide a practical approach for translating the functional and structural findings from HD experimental animal models to humans, and represent a potential tool for monitoring outcomes of disease-modifying treatments.

#### AUTHOR CONTRIBUTIONS

NG-K is the principal investigator of the IMAGE-HD study. IMAGE-HD data and image processing was conducted by PW. Statistical analyses were completed by PW and CBM. First manuscript draft was written by PW, MW, CBM, DV, and NG-K. All authors were involved in the study design, reviewing the statistical analyses, and editing of the final version of the manuscript.

#### ACKNOWLEDGMENTS

The IMAGE-HD study was supported by the CHDI Foundation Inc., New York, USA [A-3433]; and the National Health and Medical Research Council (NHMRC), Australia [606650]. Open access publishing facilitated by Monash University, as part of the Wiley - Monash University agreement via the Council of Australian University Librarians.

#### CONFLICT OF INTEREST STATEMENT

No funding was received towards this work. No financial disclosure/competing interests to declare.

#### DATA AVAILABILITY STATEMENT

The anonymized data that support the findings of this study are available from the corresponding author upon reasonable request.

#### ORCID

Pierre Wibawa  <https://orcid.org/0000-0002-7120-6984>

Charles B. Malpas  <https://orcid.org/0000-0003-0534-3718>

Nellie Georgiou-Karistianis  <https://orcid.org/0000-0003-0718-6760>

#### REFERENCES

- Goh AM, Wibawa P, Loi SM, Walterfang M, Velakoulis D, Looi JC. Huntington's disease: neuropsychiatric manifestations of Huntington's disease. *Australas Psychiatry*. 2018;26(4):366-375. doi:10.1177/1039856218791036
- Rosas HD, Salat DH, Lee SY, et al. Cerebral cortex and the clinical expression of Huntington's disease: complexity and heterogeneity. *Brain*. 2008;131(Pt 4):1057-1068. doi:10.1093/brain/awn025
- Tabrizi SJ, Langbehn DR, Leavitt BR, et al. Biological and clinical manifestations of Huntington's disease in the longitudinal TRACK-HD study: cross-sectional analysis of baseline data. *Lancet Neurol*. 2009;8(9):791-801. doi:10.1016/s1474-4422(09)70170-x
- Glikmann-Johnston Y, Fink KD, Deng P, Torrest A, Stout JC. Spatial memory in Huntington's disease: a comparative review of human and animal data. *Neurosci Biobehav Rev*. 2019;98:194-207. doi:10.1016/j.neubiorev.2019.01.015
- Possin KL, Kim H, Geschwind MD, et al. Egocentric and allocentric visuospatial working memory in premotor Huntington's disease: a double dissociation with caudate and hippocampal volumes. *Neuropsychologia*. 2017;101:57-64. doi:10.1016/j.neuropsychologia.2017.04.022
- Harris KL, Armstrong M, Swain R, et al. Huntington's disease patients display progressive deficits in hippocampal-dependent cognition during a task of spatial memory. *Cortex*. 2019;119:417-427. doi:10.1016/j.cortex.2019.07.014
- Glikmann-Johnston Y, Carmichael AM, Mercieca E-C, Stout JC. 'Real-life' hippocampal-dependent spatial memory impairments in Huntington's disease. *Cortex*. 2019;119:46-60. doi:10.1016/j.cortex.2019.04.006
- Begeti F, Schwab LC, Mason SL, Barker RA. Hippocampal dysfunction defines disease onset in Huntington's disease. *J Neurol Neurosurg Psychiatry*. 2016;87(9):975-981. doi:10.1136/jnnp-2015-312413
- van den Bogaard SJ, Dumas EM, Ferrarini L, et al. Shape analysis of subcortical nuclei in Huntington's disease, global versus local atrophy—results from the TRACK-HD study. *J Neurol Sci*. 2011;307(1-2):60-68. doi:10.1016/j.jns.2011.05.015
- Braak H, Braak E. Allocortical involvement in Huntington's disease. *Neuropathol Appl Neurobiol*. 1992;18(6):539-547. doi:10.1111/j.1365-2990.1992.tb00824.x
- Spargo E, Everall IP, Lantos PL. Neuronal loss in the hippocampus in Huntington's disease: a comparison with HIV infection. *J Neurol Neurosurg Psychiatry*. 1993;56(5):487-491. doi:10.1136/jnnp.56.5.487
- Zeineh MM, Palomero-Gallagher N, Axer M, et al. Direct visualization and mapping of the spatial course of fiber tracts at microscopic resolution in the human hippocampus. *Cereb Cortex*. 2017;27(3):1779-1794. doi:10.1093/cercor/bhw010
- O'Keefe J. A review of the hippocampal place cells. *Prog Neurobiol*. 1979;13(4):419-439. doi:10.1016/0301-0082(79)90005-4
- Robertson RG, Rolls ET, Georges-François P, Panzeri S. Head direction cells in the primate pre-subiculum. *Hippocampus*. 1999;9(3):206-219. doi:10.1002/(SICI)1098-1063(1999)9:3<206::AID-HIPO2>3.0.CO;2-H

15. Georges-François P, Rolls ET, Robertson RG. Spatial view cells in the primate hippocampus: allocentric view not head direction or eye position or place. *Cereb Cortex*. 1999;9(3):197-212. doi:10.1093/cercor/9.3.197
16. Boccarda CN, Sargolini F, Thoresen VH, et al. Grid cells in pre- and parasubiculum. *Nat Neurosci*. 2010;13(8):987-994. doi:10.1038/nn.2602
17. Vass LK, Epstein RA. Abstract representations of location and facing direction in the human brain. *J Neurosci*. 2013;33(14):6133-6142. doi:10.1523/jneurosci.3873-12.2013
18. Georgiou-Karistianis N, Gray MA, Dominguez DJF, et al. Automated differentiation of pre-diagnosis Huntington's disease from healthy control individuals based on quadratic discriminant analysis of the basal ganglia: the IMAGE-HD study. *Neurobiol Dis*. 2013;51:82-92. doi:10.1016/j.nbd.2012.10.001
19. Langbehn DR, Brinkman RR, Falush D, Paulsen JS, Hayden MR. A new model for prediction of the age of onset and penetrance for Huntington's disease based on CAG length. *Clin Genet*. 2004;65(4):267-277. doi:10.1111/j.1399-0004.2004.00241.x
20. Reuter M, Schmansky NJ, Rosas HD, Fischl B. Within-subject template estimation for unbiased longitudinal image analysis. *Neuroimage*. 2012;61(4):1402-1418. doi:10.1016/j.neuroimage.2012.02.084
21. Iglesias JE, Augustinack JC, Nguyen K, et al. A computational atlas of the hippocampal formation using ex vivo, ultra-high resolution MRI: application to adaptive segmentation of in vivo MRI. *Neuroimage*. 2015;115:117-137. doi:10.1016/j.neuroimage.2015.04.042
22. Sämann PG, Iglesias JE, Gutman B, et al. FreeSurfer-based segmentation of hippocampal subfields: a review of methods and applications, with a novel quality control procedure for ENIGMA studies and other collaborative efforts. *Hum Brain Mapp*. 2020;43(1):207-233. doi:10.1002/hbm.25326
23. Fedorov A, Beichel R, Kalpathy-Cramer J, et al. 3D slicer as an image computing platform for the quantitative imaging network. *Magn Reson Imaging*. 2012;30(9):1323-1341. doi:10.1016/j.mri.2012.05.001
24. Moeller J. A word on standardization in longitudinal studies: don't. *Front Psychol*. 2015;6:1389. doi:10.3389/fpsyg.2015.01389
25. Beaujoin J, Palomero-Gallagher N, Boumezbaur F, et al. Post-mortem inference of the human hippocampal connectivity and microstructure using ultra-high field diffusion MRI at 11.7 T. *Brain Struct Funct*. 2018;223(5):2157-2179. doi:10.1007/s00429-018-1617-1
26. Rolls ET. Neurons including hippocampal spatial view cells, and navigation in primates including humans. *Hippocampus*. 2021;31(6):593-611. doi:10.1002/hipo.23324
27. Insausti R, Muñoz-López M, Insausti AM, Artacho-Pérola E. The human periallocortex: layer pattern in presubiculum, parasubiculum and entorhinal cortex. A review. *Front Neuroanat*. 2017;11:84. doi:10.3389/fnana.2017.00084
28. Dalton MA, Zeidman P, Barry DN, Williams E, Maguire EA. Segmenting subregions of the human hippocampus on structural magnetic resonance image scans: an illustrated tutorial. *Brain Neurosci Adv*. 2017;1:2398212817701448. doi:10.1177/2398212817701448
29. Klausberger T, Somogyi P. Neuronal diversity and temporal dynamics: the unity of hippocampal circuit operations. *Science*. 2008;321(5885):53-57. doi:10.1126/science.1149381
30. Pignatelli M, Lebreton F, Cho YH, Leinekugel X. "Ectopic" theta oscillations and interictal activity during slow-wave state in the R6/1 mouse model of Huntington's disease. *Neurobiol Dis*. 2012;48(3):409-417. doi:10.1016/j.nbd.2012.07.015
31. Bylsma FW, Peyser CE, Folstein SE, Ross C, Brandt J. EEG power spectra in huntington's disease: clinical and neuropsychological correlates. *Neuropsychologia*. 1994;32(2):137-150. doi:10.1016/0028-3932(94)90001-9
32. Gutekunst C-A, Li S-H, Yi H, et al. Nuclear and neuropil aggregates in Huntington's disease: relationship to neuropathology. *J Neurosci*. 1999;19(7):2522-2534. doi:10.1523/jneurosci.19-07-02522.1999
33. Reiner A, Shelby E, Wang H, et al. Striatal parvalbuminergic neurons are lost in Huntington's disease: implications for dystonia. *Mov Disord*. 2013;28(12):1691-1699. doi:10.1002/mds.25624
34. Kim EH, Thu DCV, Tippett LJ, et al. Cortical interneuron loss and symptom heterogeneity in Huntington disease. *Ann Neurol*. 2014;75(5):717-727. doi:10.1002/ana.24162
35. Brady DR, Mufson EJ. Parvalbumin-immunoreactive neurons in the hippocampal formation of Alzheimer's diseased brain. *Neuroscience*. 1997;80(4):1113-1125. doi:10.1016/s0306-4522(97)00068-7
36. Waldvogel HJ, Faull RLM. Chapter 9-The diversity of GABAA receptor subunit distribution in the normal and Huntington's disease human brain. *Adv Pharmacol*. 2015;73:223-264. doi:10.1016/bs.apha.2014.11.010
37. Palomero-Gallagher N, Kedo O, Mohlberg H, Zilles K, Amunts K. Multimodal mapping and analysis of the cyto- and receptorarchitecture of the human hippocampus. *Brain Struct Funct*. 2020;225(3):881-907. doi:10.1007/s00429-019-02022-4
38. Barron JC, Hurley EP, Parsons MP. Huntingtin and the synapse. *Front Cell Neurosci*. 2021;15(225):689332. doi:10.3389/fncel.2021.689332
39. von Hörsten S, Schmitt I, Nguyen HP, et al. Transgenic rat model of Huntington's disease. *Hum Mol Genet*. 2003;12(6):617-624. doi:10.1093/hmg/ddg075
40. Sathasivam K, Lane A, Legleiter J, et al. Identical oligomeric and fibrillar structures captured from the brains of R6/2 and knock-in mouse models of Huntington's disease. *Hum Mol Genet*. 2009;19(1):65-78. doi:10.1093/hmg/ddp467
41. Landles C, Milton RE, Ali N, et al. Subcellular localization and formation of huntingtin aggregates correlates with symptom onset and progression in a Huntington's disease model. *Brain Commun*. 2020;2(2):fcaa066. doi:10.1093/braincomms/fcaa066
42. Lange KW, Javoy-Agid F, Agid Y, Jenner P, Marsden CD. Brain muscarinic cholinergic receptors in Huntington's disease. *J Neurol*. 1992;239(2):103-104. doi:10.1007/BF00862983
43. Bauer A, Zilles K, Matusch A, Holzmann C, Riess O, von Hörsten S. Regional and subtype selective changes of neurotransmitter receptor density in a rat transgenic for the Huntington's disease mutation. *J Neurochem*. 2005;94(3):639-650. doi:10.1111/j.1471-4159.2005.03169.x
44. Ding S-L. Comparative anatomy of the prosubiculum, subiculum, presubiculum, postsubiculum, and parasubiculum in human, monkey, and rodent. *J Comp Neurol*. 2013;521(18):4145-4162. doi:10.1002/cne.23416
45. Schwab LC, Richetin K, Barker RA, Déglon N. Formation of hippocampal mHTT aggregates leads to impaired spatial memory, hippocampal activation and adult neurogenesis. *Neurobiol Dis*. 2017;102:105-112. doi:10.1016/j.nbd.2017.03.005
46. Espinoza C, Guzman SJ, Zhang X, Jonas P. Parvalbumin+ interneurons obey unique connectivity rules and establish a powerful lateral-inhibition microcircuit in dentate gyrus. *Nat Commun*. 2018;9(1):4605. doi:10.1038/s41467-018-06899-3
47. Gratuze M, Cisbani G, Cicchetti F, Planel E. Is Huntington's disease a tauopathy? *Brain*. 2016;139(Pt 4):1014-1025. doi:10.1093/brain/aww021
48. L'Episcopo F, Drouin-Ouellet J, Tirolo C, et al. GSK-3β-induced tau pathology drives hippocampal neuronal cell death in Huntington's disease: involvement of astrocyte-neuron interactions. *Cell Death Dis*. 2016;7(4):e2206. doi:10.1038/cddis.2016.104
49. Langbehn DR, Stout JC, Gregory S, et al. Association of CAG repeats with long-term progression in Huntington disease. *JAMA Neurol*. 2019;76(11):1375-1385. doi:10.1001/jamaneurol.2019.2368
50. Ferrari Bardile C, Garcia-Mirallas M, Caron NS, et al. Intrinsic mutant HTT-mediated defects in oligodendroglia cause myelination deficits

and behavioral abnormalities in Huntington disease. *Proc Natl Acad Sci.* 2019;116(19):9622-9627. doi:[10.1073/pnas.1818042116](https://doi.org/10.1073/pnas.1818042116)

## SUPPORTING INFORMATION

Additional supporting information can be found online in the Supporting Information section at the end of this article.

**How to cite this article:** Wibawa P, Walterfang M, Malpas CB, et al. Selective perforant-pathway atrophy in Huntington disease: MRI analysis of hippocampal subfields. *Eur J Neurol.* 2023;30:2650-2660. doi:[10.1111/ene.15918](https://doi.org/10.1111/ene.15918)